



Coherent quantum annealing in a programmable 2,000 qubit Ising chain

Andrew D. King¹, Sei Suzuki², Jack Raymond¹, Alex Zucca¹, Trevor Lanting¹, Fabio Altomare¹, Andrew J. Berkley¹, Sara Ejtemaee¹, Emile Hoskinson¹, Shuiyuan Huang¹, Eric Ladizinsky¹, Allison J. R. MacDonald¹, Gaelen Marsden¹, Travis Oh¹, Gabriel Poulin-Lamarre¹, Mauricio Reis¹, Chris Rich¹, Yuki Sato¹, Jed D. Whittaker¹, Jason Yao¹, Richard Harris¹, Daniel A. Lidar^{3,4}, Hidetoshi Nishimori^{5,6,7} and Mohammad H. Amin^{1,8}

Quantum simulation has emerged as a valuable arena for demonstrating and understanding the capabilities of near-term quantum computers1-3. Quantum annealing4,5 has been successfully used in simulating a range of open quantum systems, both at equilibrium⁶⁻⁸ and out of equilibrium⁹⁻¹¹. However, in all previous experiments, annealing has been too slow to coherently simulate a closed quantum system, due to the onset of thermal effects from the environment. Here we demonstrate coherent evolution through a quantum phase transition in the paradigmatic setting of a one-dimensional transverse-field Ising chain, using up to 2,000 superconducting flux qubits in a programmable quantum annealer. In large systems, we observe the quantum Kibble-Zurek mechanism with theoretically predicted kink statistics, as well as characteristic positive kink-kink correlations, independent of temperature. In small chains, excitation statistics validate the picture of a Landau-Zener transition at a minimum gap. In both cases, the results are in quantitative agreement with analytical solutions to the closed-system quantum model. For slower anneals, we observe anti-Kibble-Zurek scaling in a crossover to the open quantum regime. The coherent dynamics of large-scale quantum annealers demonstrated here can be exploited to perform approximate quantum optimization, machine learning and simulation tasks.

Quantum phase transitions (QPTs) describe the sudden macroscopic change in a system's ground state driven by quantum fluctuations¹². An important aspect of phase transitions is the divergence of correlation length ξ at the critical point, resulting in a universal behaviour: macroscopic properties become independent of the Hamiltonian details. The growth of correlation length happens within response time τ , which also diverges at the critical point due to critical slowing down. For a finite system, the correlation length is limited by system size. Therefore, a slow quench through a QPT, that is, within a time longer than τ , can adiabatically transition the system into its new ground state¹³. Outside the adiabatic regime, the correlation length remains shorter than the system size, leading to defects, that is, boundaries between domains with different orders. The average distance between the defects is set by the correlation

length, which itself is a function of quench velocity. The defect density scales polynomially with the speed at which the critical point is traversed. This phenomenon, known as the Kibble–Zurek mechanism (KZM)¹⁴, has its origins in the cosmology of the early Universe, but has since been observed in various experimental platforms such as Bose–Einstein condensates^{15,16}, Rydberg atoms^{3,17} and trapped ions¹⁸.

The quantum Ising chain is a popular testbed for studying the KZM^{3,19-24} in part because it can be exactly solved using fermionization via the Jordan–Wigner transformation²⁰. We implement this model using a programmable superconducting quantum annealer (QA)⁵. The Hamiltonian of this system is given by

$$H(s) = -\Gamma(s) \sum_{i=1}^{L} \sigma_i^x + \mathcal{J}(s) \sum_{i=1}^{L} J \sigma_i^z \sigma_{i+1}^z, \tag{1}$$

where σ_i^z and σ_i^x are Pauli operators on the ith qubit and J is a dimensionless programmable coupling. For annealing time t_a , the annealing parameter $s=t/t_a$ ranges from 0 to 1, controlling the transverse field $\Gamma(s)$ and Ising energy scale $\mathcal{J}(s)$ according to the schedule depicted in Fig. 1a (Supplementary Information shows the detailed modelling in which we determine the schedule terms $\Gamma(s)$ and $\mathcal{J}(s)$ for each programmed value of J based on a radio-frequency superconducting quantum interference device flux qubit model). We use periodic boundary conditions ($\sigma_{L+1}^a = \sigma_1^a$) and program all the couplers with the same value J, which can be either positive (antiferromagnetic) or negative (ferromagnetic).

In the paramagnetic phase, when $s \approx 0$, the system is dominated by quantum fluctuations and the ground state is an approximately uniform superposition of computational basis states (eigenstates of σ_i^z). At the end of annealing, when s=1, the system is diagonal in the computational basis, with frozen dynamics. This ordered phase has a ferromagnetic ground state; these two phases are separated by a quantum critical point at $s=s_c$ such that $\Gamma(s_c)=\mathcal{J}(s_c)|J|$ (Fig. 1b).

To probe kink density scaling in the thermodynamic limit, we anneal chains of L = 512 and 2,000 qubits for varying t_a , at qubit temperatures between 10 and 30 mK and for several values of J

¹D-Wave Systems, Burnaby, British Columbia, Canada. ²Department of Liberal Arts, Saitama Medical University, Moroyama, Japan. ³Departments of Electrical and Computer Engineering, Chemistry, Physics & Astronomy, University of Southern California, Los Angeles, CA, USA. ⁴Center for Quantum Information Science & Technology (CQIST), University of Southern California, Los Angeles, CA, USA. ⁵International Research Frontiers Initiative, Tokyo Institute of Technology, Tokyo, Japan. ⁶Graduate School of Information Sciences, Tohoku University, Sendai, Japan. ⁷Interdisciplinary Theoretical and Mathematical Sciences, RIKEN, Wako, Japan. ⁸Department of Physics, Simon Fraser University, Burnaby, British Columbia, Canada.

NATURE PHYSICS LETTERS

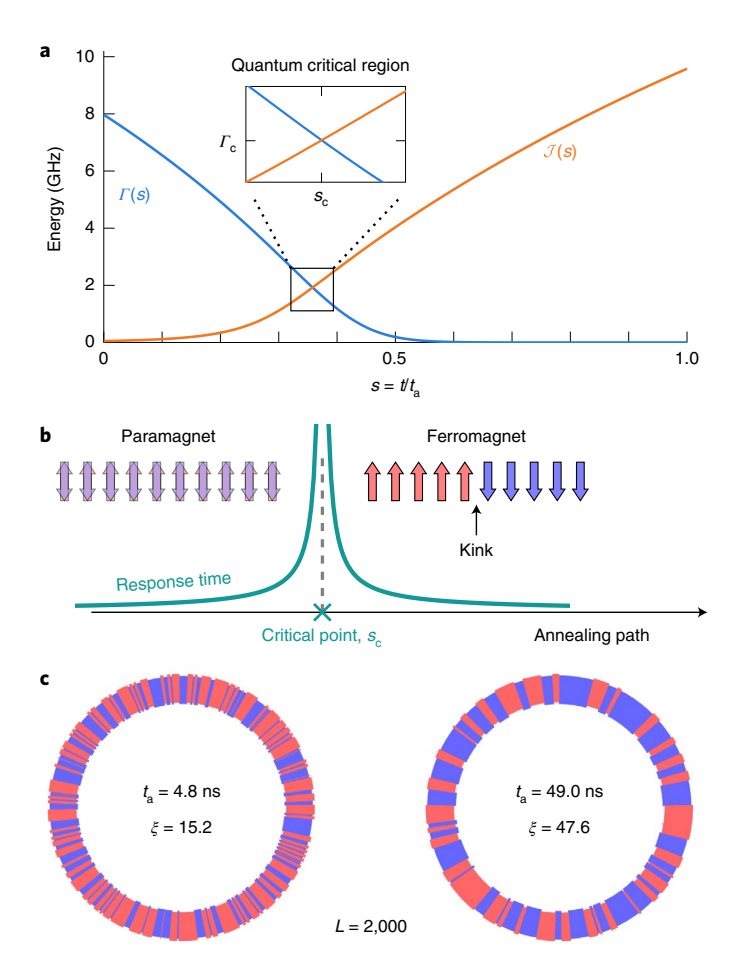


Fig. 1 | QPT in an annealed Ising chain. a, Quantum annealing of the transverse-field Ising chain. Using a dimensionless annealing parameter s to control the Hamiltonian in equation (1) with J=1, the system is tuned through its QPT at $\Gamma(s_c)=\mathcal{J}(s_c)$ for $s_c\approx 0.36$. The critical point separates a quantum paramagnet ($s< s_c$) from an ordered ground state ($s> s_c$). **b**, Response time diverges at the quantum critical point, as a function $\tau \propto |s-s_c|^{-\tau \nu}$ for critical exponents z and ν . Consequently, a finite-time traversal of the QPT results in kinks separating ordered domains after annealing. **c**, Example QA output states for a chain of L=2,000 qubits with J=-1.4, whose alternating domains of up (red) and down (blue) spins have correlation length $\xi=1/\bar{n}$, where \bar{n} is the average kink density.

ranging in magnitude from 0.12 to 1.40. Figure 1c shows examples of experimental data from the QA for $t_{\rm a}$ =4.8 and 49.0 ns with J=-1.4. As expected from the KZM, longer annealing exhibits fewer kinks. We define the kink operator as

$$K_i = \left[1 + \operatorname{sign}(J)\sigma_i^z \sigma_{i+1}^z\right]/2. \tag{2}$$

At the end of annealing, when all the qubits are measured in the computational basis, $K_i=1$ if there is a kink between qubits i and i+1, and $K_i=0$ otherwise. We define the kink density operator as

$$n = \frac{1}{L} \sum_{i=1}^{L} K_{i}.$$
 (3)

The average kink density $\bar{n} = \langle n \rangle$ is obtained by running the experiment many times and averaging over the outcomes. Measurements of \bar{n} are summarized in Fig. 2a. To test the ability of L=512 to represent the thermodynamic limit, we confirmed consistency

with L=2,000 at 10 mK. For $t_a \ge 1\,\mu s$, \bar{n} decreases monotonically as a function of t_a , consistent with previous experiments in the same regime¹⁰. For the previously unexplored region $t_a < 1\,\mu s$, \bar{n} is non-monotonic, particularly for high temperature and weak coupling. This 'anti-Kibble–Zurek' behaviour is a result of coupling to a thermal environment, which generates additional excitations and thus increases \bar{n} ; such a behaviour has been seen in the classical simulations of open-system quantum Ising chains^{10,23} and two-dimensional systems in a OA outside the coherent regime¹¹.

For the shortest anneals, kink densities at all the temperatures collapse on a common curve. This temperature independence is the evidence of coherent evolution, where the system traverses the quantum critical point faster than the environment's response time. In this case, the system is unable to exchange energy with the environment. The exactly solvable coherent (closed-system) quantum model predicts^{20,25} (Supplementary Information)

$$\bar{n} = \frac{t_{\rm a}^{-1/2}}{2\pi\sqrt{2b}}, \quad b = \frac{\Gamma(s_{\rm c})/\hbar}{\mathcal{J}'(s_{\rm c})/\mathcal{J}(s_{\rm c}) - \Gamma'(s_{\rm c})/\Gamma(s_{\rm c})},$$
 (4)

where h is the reduced Planck constant. This theoretical kink density (Fig. 2a, dashed lines) is in quantitative agreement with the experimental measurements in the fast-annealing regime, with no fitting parameters.

Kink distributions in the quantum Ising chain have been theoretically characterized beyond just the average densities. The number of kinks follows a binomial distribution 24 ; when the number of kinks is large, this distribution is well approximated by a Gaussian distribution. This clearly differentiates the data from a Boltzmann distribution describing thermal equilibrium (Fig. 2b). Unlike a Gaussian distribution, the binomial kink distribution is expected to skew slightly away from zero and therefore have a positive third cumulant. Moreover, the first three cumulants of the kink distribution, namely, $\kappa_1=\bar{n},\ \kappa_2=\langle(n-\bar{n})^2\rangle$ and $\kappa_3=\langle(n-\bar{n})^3\rangle$, are expected to be proportional to $t_a^{-1/2}$, at fixed ratios 24

$$\kappa_2/\kappa_1 = 2 - \sqrt{2} \approx 0.586,\tag{5}$$

$$\kappa_3/\kappa_1 = 4(1 - 3/\sqrt{2} + 2/\sqrt{3}) \approx 0.134.$$
(6)

Measurements of these cumulants are shown in Fig. 2c. The lines in the figure are derived from theory, showing good agreement with the experimental data.

Although single-point QA statistics agree with the closed-system quantum model, some aspects of the kink distribution can be reproduced by classical models²⁶. For example, the scaling exponent of -1/2 (equation (4)) is identical to that of a purely classical diffusion/annihilation model²⁷. Therefore, we investigate two-point statistics^{28,29}. We define the normalized kink–kink correlator as

$$C_r^{KK} = \frac{1}{L} \sum_{i=1}^{L} \frac{\langle K_i K_{i+r} \rangle - \bar{n}^2}{\bar{n}^2}.$$
 (7)

In Fig. 3a, we plot $C_r^{\rm KK}$ against the normalized lattice distance $r/\xi = \bar{n}r$. For multiple annealing times, the data collapse on a curve with a positive peak at around $r/\xi \approx 0.6$, as predicted elsewhere²⁹. The QA data are compared with the solution of the fermionized model (Fig. 3b), which exhibits a similar but higher peak.

Peak suppression in QA is expected from coarsening dynamics²⁸ or other mechanisms such as dephasing²⁹ or kink diffusion outside the regime of validity of the adiabatic/impulse description of KZM. Indeed, $C_r^{\rm KK}$ does become purely negative for longer anneals (Supplementary Fig. 15). However, thermal effects do not appear to play a role (Supplementary Fig. 14). To probe the potential effects of

LETTERS NATURE PHYSICS

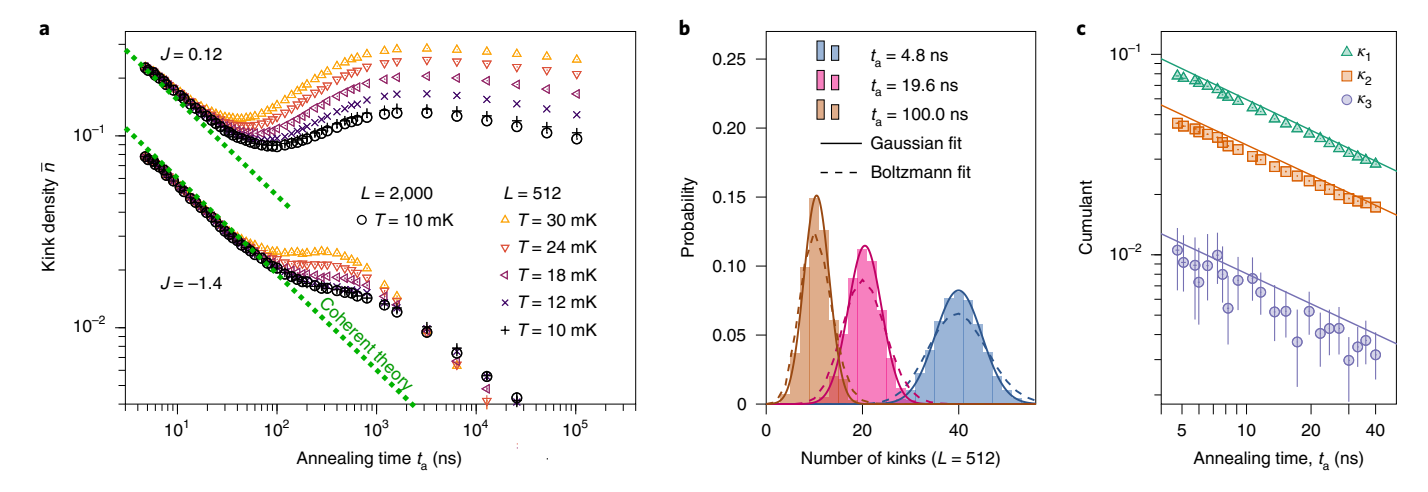


Fig. 2 | Kink density scaling and distribution. a, QA data for weak coupling (J=0.12) and strong coupling (J=-1.4, used for **b** and **c**) for a range of temperatures and annealing times. The weak coupling regime exhibits anti-Kibble–Zurek behaviour, with a local minimum in \bar{n} . For strong coupling and fast anneals, \bar{n} is unaffected by temperature and quantitatively agrees with the closed-system coherent quantum theory (dotted green lines; equation (4)). **b**, Best-fit thermal (Boltzmann) model is significantly broader than the measurement results, which are better described by a Gaussian model, as expected given the predicted binomial form. **c**, First three cumulants of the kink distribution. The lines indicate coherent theory. The markers and error bars indicate the bootstrap mean and 95% statistical confidence intervals, respectively (Methods).

entanglement and disorder, we employ a tensor-network dynamics method known as time-evolution block decimation (TEBD)³⁰. Reducing the TEBD bond dimension D (Supplementary Section E) to 20 provides a heuristic model of limited entanglement entropy S, given that $S \le 2\log(D)$ (ref. ³¹); this slightly lowers the peak (Fig. 3c), but makes it dependent on t_a , inconsistent with the experimental data. Further lowering D worsens the agreement with QA (Supplementary Fig. 9), but combining D=20 with disorder in the QA Hamiltonian improves it (Supplementary Information). Combining these effects gives a close match to the QA results for J=-1.4 (Fig. 3d) and other coupling strengths (Supplementary Fig. 10). Moreover, we find that D=20 is a lower bound on the bond dimension, in the sense that our QA data display an opposite trend with t_a to that of TEBD for D < 20, but our QA and TEBD data agree for $D \ge 20$ (Supplementary Fig. 16).

Previous studies have shown logarithmic, rather than power-law, scaling of \bar{n} in the presence of large disorder, with J_i uniformly sampled in $[0, J_{\text{max}}]$ (refs. ^{32,33}). Although the much smaller disorder probed in Fig. 3d (σ =0.05) substantially suppresses the peak in C_r^{KK} , the effect on kink density is small, especially for fast anneals where \bar{n} is large (Supplementary Fig. 11). Furthermore, the disorder in this case arises from technical challenges in QA, which are the most severe for fast anneals. Therefore, a significant region of power-law scaling, as seen in our experimental results (Fig. 2a), is consistent with our understanding of disorder.

Next, we investigate finite-size effects. When t_a is sufficiently large as a function of L, the dynamics are dominated by a single Landau–Zener (LZ) transition³⁴, and the ground-state probability P_{GS} follows the adiabatic theorem³⁵. This crossover occurs when $L\bar{n}\approx 1$ (ref. ³³). The LZ transition probability is expected to exponentially decay in the annealing time, in contrast to the power-law dependence in the Kibble–Zurek regime. For one-dimensional spin chains, it is possible to obtain an analytical solution²⁰ (Supplementary Information):

$$1 - P_{GS} = e^{-at_a}, \quad a = 2\pi^3 b L^{-2}, \tag{8}$$

where b is defined in equation (4).

Figure 4a shows the QA measurements for ferromagnetic and antiferromagnetic chains of equal coupling magnitude $(J=\pm 0.95)$. Since L is even, the two Ising Hamiltonians are gauge equivalent

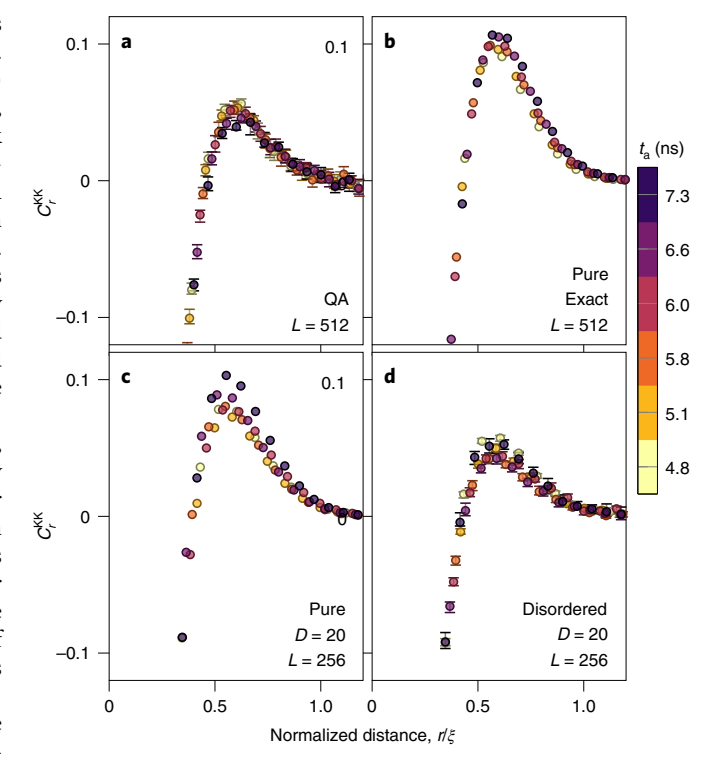


Fig. 3 | Normalized kink-kink correlations. a, QA data with J=-1.4 (left) have a positive peak in C_r^{KK} , which are compared with closed-system quantum models. **b**, Exact time evolution of the fermionized model. **c**, TEBD with limited bond dimension D=20. **d**, TEBD with D=20 and $\sigma=0.05$ Gaussian disorder added to the longitudinal fields and couplings. All the models have $C_r^{KK} \rightarrow -1$ as $r/\xi \rightarrow 0$. The markers and error bars in **a** and **d** indicate the bootstrap mean and 95% statistical confidence intervals, respectively, across experiments and disorder realizations.

and we expect similar experimental outcomes. We plot the data in the range $5 \le t_a \le 40$ ns and $0.1 \le P_{GS} \le 0.9$ for values of L ranging from 8 to 32. Figure 4a also shows the results of the exact

NATURE PHYSICS LETTERS

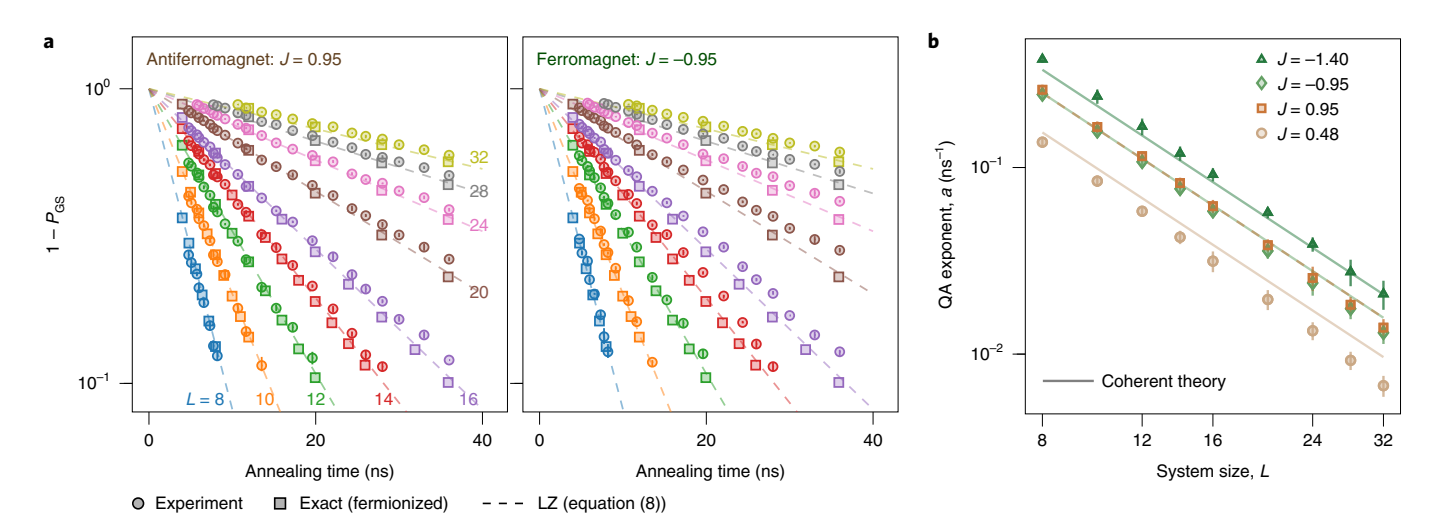


Fig. 4 | Crossover to adiabaticity. a, QA data (circles) for antiferromagnetic (left) and ferromagnetic (right) chains are compared with exact closed-system numerics (squares), using an independently extracted annealing schedule based on single-qubit measurements. Both closely agree with the LZ model of diabatic transition occurring at the minimum gap (dashed lines; equation (8)). **b**, Exponent *a* extracted from the QA data in **a** for different *J* and *L* values. The solid lines are analytical values from the closed-system model. The markers and error bars indicate the bootstrap mean and 95% confidence intervals, respectively (Methods).

simulation of coherent Schrödinger dynamics for the fermionized system (squares; Supplementary Information) together with the analytical result of equation (8) (dashed lines), in remarkable agreement with the experimental data. To test the agreement with the closed-system theory for different J values, Fig. 4b shows that a as extracted from the empirical $P_{\rm GS}$ data as per equation (8) remains consistent with the theoretical prediction of $a \propto L^{-2}$ (solid lines).

Although all the above experimental results agree well with coherent quantum dynamics, an important question is whether they can also be explained by classical models. It is clearly impractical and even impossible to rule out every classical explanation; instead, we consider the most plausible Monte Carlo methods that have been suggested as emulators for QA^{36,37}. In Supplementary Section B, we consider simulated annealing, simulated quantum annealing based on path-integral Monte Carlo and spin-vector Monte Carlo simulations. We find that some of these models can reproduce some aspects of the experimental data, but none of them can explain all the experimental features. Therefore, we conclude that only the coherent quantum model successfully explains all the experimental results, and this view is considerably strengthened by the fact that we have not used any fitting parameters.

In conclusion, by tuning the parameters of a programmable QA, namely, annealing time, coupling strength and temperature, we have simulated quantum critical phenomena in one-dimensional chains of up to 2,000 spins. For fast anneals, we observe quantum Kibble-Zurek scaling in long chains and LZ scaling in short chains. In both regimes, kink densities are in quantitative agreement with coherent Schrödinger dynamics-remarkably, with no free parameters. In contrast, leading classical models can only reproduce some aspects of the experimental data—no single classical theory reproduces all of them. These results represent strong evidence for coherent evolution, with a significantly larger system and longer correlation length $(L=2,000, \xi \approx 30)$ than previous quantum Kibble–Zurek demonstrations in a one-dimensional system using Rydberg arrays (L=51, $\xi \approx 4$)³. In addition, at longer annealing times, we observe a crossover to the thermal regime with anti-Kibble-Zurek behaviour, as theoretically predicted¹⁰.

We have used QA as a quantum simulator, producing results that are challenging to simulate classically, even in this widely studied and simple model. Path-integral Monte Carlo simulations can simulate systems near thermal equilibrium³⁸, but cannot be used to describe or simulate quantum dynamics^{39–41}. Likewise, open-system quantum simulations such as master equations⁴² become computationally intractable beyond system sizes of around 40 qubits. Thus, our results pave the way to coherent quantum simulation on a previously unattainable scale. Moreover, the ability to program both signs and magnitudes of Hamiltonian terms in a coherently evolved system is a key ingredient in the simulation of frustrated models such as quantum spin glasses and ultimately in quantum optimization. The results reported here represent an important step towards this goal.

Online content

Any methods, additional references, Nature Research reporting summaries, source data, extended data, supplementary information, acknowledgements, peer review information; details of author contributions and competing interests; and statements of data and code availability are available at https://doi.org/10.1038/s41567-022-01741-6.

Received: 15 February 2022; Accepted: 28 July 2022; Published online: 15 September 2022

References

- Kandala, A. et al. Hardware-efficient variational quantum eigensolver for small molecules and quantum magnets. *Nature* 549, 242–246 (2017).
- Zhang, J. et al. Observation of a many-body dynamical phase transition with a 53-qubit quantum simulator. Nature 551, 601-604 (2017).
- Keesling, A. et al. Quantum Kibble–Zurek mechanism and critical dynamics on a programmable Rydberg simulator. *Nature* 568, 207–211 (2019).
- Kadowaki, T. & Nishimori, H. Quantum annealing in the transverse Ising model. Phys. Rev. E 58, 5355 (1998).
- Johnson, M. W. et al. Quantum annealing with manufactured spins. Nature 473, 194–198 (2011).
- Harris, R. et al. Phase transitions in a programmable quantum spin glass simulator. Science 361, 162–165 (2018).
- King, A. D. et al. Observation of topological phenomena in a programmable lattice of 1,800 qubits. *Nature* 560, 456–460 (2018).
- Nishimura, K., Nishimori, H. & Katzgraber, H. G. Griffiths-McCoy singularity on the diluted Chimera graph: Monte Carlo simulations and experiments on quantum hardware. *Phys. Rev. A* 102, 042403 (2020).
- 9. Gardas, B., Dziarmaga, J., Zurek, W. H. & Zwolak, M. Defects in quantum computers. Sci. Rep. 8, 4539 (2018).

LETTERS NATURE PHYSICS

- Bando, Y. et al. Probing the universality of topological defect formation in a quantum annealer: Kibble-Zurek mechanism and beyond. *Phys. Rev. Res.* 2, 033369 (2020).
- 11. Weinberg, P. et al. Scaling and diabatic effects in quantum annealing with a D-Wave device. *Phys. Rev. Lett.* **124**, 090502 (2020).
- 12. Dutta, A. et al. Quantum Phase Transitions in Transverse Field Spin Models: From Statistical Physics to Quantum Information (Cambridge Univ. Press, 2015).
- 13. Albash, T. & Lidar, D. A. Adiabatic quantum computation. Rev. Mod. Phys. 90, 015002 (2018).
- Zurek, W. H. Cosmological experiments in superfluid helium? Nature 317, 505–508 (1985).
- 15. Anquez, M. et al. Quantum Kibble-Zurek mechanism in a spin-1 Bose-Einstein condensate. *Phys. Rev. Lett.* **116**, 155301 (2016).
- Clark, L. W., Feng, L. & Chin, C. Universal space-time scaling symmetry in the dynamics of bosons across a quantum phase transition. *Science* 354, 606–610 (2016)
- Browaeys, A. & Lahaye, T. Many-body physics with individually controlled Rydberg atoms. Nat. Phys. 16, 132–142 (2020).
- Cui, J. M. et al. Experimentally testing quantum critical dynamics beyond the Kibble–Zurek mechanism. Commun. Phys. 3, 44 (2020).
- 19. Zurek, W. H., Dorner, U. & Zoller, P. Dynamics of a quantum phase transition. *Phys. Rev. Lett.* **95**, 105701 (2005).
- Dziarmaga, J. Dynamics of a quantum phase transition: exact solution of the quantum Ising model. *Phys. Rev. Lett.* 95, 245701 (2005).
- Polkovnikov, A. Universal adiabatic dynamics in the vicinity of a quantum critical point. Phys. Rev. B 72, 161201 (2005).
- Cincio, L., Dziarmaga, J., Meisner, J. & Rams, M. M. Dynamics of a quantum phase transition with decoherence: quantum Ising chain in a static spin environment. *Phys. Rev. B* 79, 094421 (2009).
- Arceci, L., Barbarino, S., Rossini, D. & Santoro, G. E. Optimal working point in dissipative quantum annealing. *Phys. Rev. B* 98, 064307 (2018).
- 24. del Campo, A. Universal statistics of topological defects formed in a quantum phase transition. *Phys. Rev. Lett.* **121**, 200601 (2018).
- Cherng, R. W. & Levitov, L. S. Entropy and correlation functions of a driven quantum spin chain. *Phys. Rev. A* 73, 043614 (2006).
- Mayo, J. J., Fan, Z., Chern, G.-W. & del Campo, A. Distribution of kinks in an Ising ferromagnet after annealing and the generalized Kibble-Zurek mechanism. *Phys. Rev. Res.* 3, 033150 (2021).
- Krebs, K., Pfannmüller, M. P., Wehefritz, B. & Hinrichsen, H. Finite-size scaling studies of one-dimensional reaction-diffusion systems. Part I. Analytical results. J. Stat. Phys. 78, 1429–1470 (1995).
- Roychowdhury, K., Moessner, R. & Das, A. Dynamics and correlations at a quantum phase transition beyond Kibble-Zurek. *Phys. Rev. B* 104, 014406 (2021).

- Nowak, R. J. & Dziarmaga, J. Quantum Kibble-Zurek mechanism: kink correlations after a quench in the quantum Ising chain. *Phys. Rev. B* 104, 075448 (2021).
- Oshiyama, H., Shibata, N. & Suzuki, S. Kibble–Zurek mechanism in a dissipative transverse Ising chain. J. Phys. Soc. Jpn 89, 104002 (2020).
- Schuch, N., Wolf, M. M., Verstraete, F. & Cirac, J. I. Entropy scaling and simulability by matrix product states. *Phys. Rev. Lett.* 100, 030504 (2008).
- 32. Dziarmaga, J. Dynamics of a quantum phase transition and relaxation to a steady state. *Adv. Phys.* **59**, 1063–1189 (2010).
- Zanca, T. & Santoro, G. E. Quantum annealing speedup over simulated annealing on random Ising chains. *Phys. Rev. B* 93, 224431 (2016).
- Zener, C. Non-adiabatic crossing of energy levels. Proc. R. Soc. Lond. A 137, 696–702 (1932).
- Kato, T. On the adiabatic theorem of quantum mechanics. J. Phys. Soc. Jpn 5, 435–439 (1950).
- Isakov, S. V. et al. Understanding quantum tunneling through quantum Monte Carlo simulations. *Phys. Rev. Lett.* 117, 180402 (2016).
- Mazzola, G., Smelyanskiy, V. N. & Troyer, M. Quantum Monte Carlo tunneling from quantum chemistry to quantum annealing. *Phys. Rev. B* 96, 134305 (2017).
- 38. Suzuki, M. Relationship between *d*-dimensional quantal spin systems and (*d*+1)-dimensional Ising systems: equivalence, critical exponents and systematic approximants of the partition function and spin correlations. *Prog. Theor. Phys.* **56**, 1454–1469 (1976).
- Liu, C. W., Polkovnikov, A. & Sandvik, A. W. Quantum versus classical annealing: insights from scaling theory and results for spin glasses on 3-regular graphs. *Phys. Rev. Lett.* 114, 147203 (2015).
- King, A. D. et al. Scaling advantage over path-integral Monte Carlo in quantum simulation of geometrically frustrated magnets. *Nat. Commun.* 12, 1113 (2021).
- 41. Bando, Y. & Nishimori, H. Simulated quantum annealing as a simulator of nonequilibrium quantum dynamics. *Phys. Rev. A* **104**, 022607 (2021).
- Yip, K. W., Albash, T. & Lidar, D. A. Quantum trajectories for time-dependent adiabatic master equations. *Phys. Rev. A* 97, 022116 (2018).

Publisher's note Springer Nature remains neutral with regard to jurisdictional claims in published maps and institutional affiliations.

Springer Nature or its licensor holds exclusive rights to this article under a publishing agreement with the author(s) or other rightsholder(s); author self-archiving of the accepted manuscript version of this article is solely governed by the terms of such publishing agreement and applicable law.

© The Author(s), under exclusive licence to Springer Nature Limited 2022

NATURE PHYSICS LETTERS

Methods

Quantum annealing experiments. Quantum annealing is performed on a D-Wave 2000Q lower-noise processor using multiple randomly generated embeddings (one for L = 2,000, three for L = 512 and up to 100 for L = 8) in parallel. Each data point represents data taken over 300 iterations for L = 2,000 and L = 512, and 50 iterations for smaller values of L. In each iteration, the qubits are annealed 100 times, providing 100 spin states. Each spin state consists of values $\{s_i\}_{i=1}^L$, where s_i = ± 1 is the qubit readout state in the computational basis.

For each data point in the plots, we refine the general-purpose calibration by fine-tuning individual Hamiltonian terms based on trivial symmetries of the chain: we tune the per-qubit linear flux biases to bring qubits to degeneracy ($\langle s_i \rangle \approx 0$), and tune two-qubit couplers to homogenize average correlations across chain bonds ($\langle s_i \rangle \approx \sum_{(k,c)} \langle s_i s_c \rangle / L$), as shown in previous studies of degenerate systems^{7,8}. To mitigate the desynchronization of annealing schedules between different qubits for the fastest anneals, we additionally refine the annealing offsets based on annealing lines, although in this case, there is little effect. We describe these methods in the Supplementary Information.

To generate error bars, a statistical bootstrap is performed. For individual data points, the method treats each QPU call as an individual trial and resamples with replacement. In particular, estimates of $C_r^{\rm KK}$ are computed for each QPU call and then bootstrapped; therefore, each estimate of \bar{n} represents a QPU call, not an overall average. The error bars in Figs. 2, 3 and 4a indicate 95% confidence intervals over QPU programming (or in Fig. 3d for over 300 disorder realizations).

To compute QA exponents a (Fig. 4b), we treat every $t_{\rm a}$ as a trial, and generate a distribution of fit slopes based on bootstrapped sets of annealing times. The data markers and error bars represent the median and 95% confidence interval of the resampling median.

Annealing schedule. The annealing schedule (Fig. 1) is based on qubit parameters extracted through averaged single-qubit measurements. Since qubits are actually multilevel objects rather than perfect two-level Ising spins, we convert the qubit Hamiltonian to an effective Ising Hamiltonian following the method laid out in recent studies of geometrically frustrated lattices 40 . We perform the approximate diagonalization of the s-dependent eigenspectrum of a 12 qubit periodic-chain Hamiltonian. We simplify the computation by dividing the qubits into four chains of three qubits each, and retaining only the 12 lowest energy levels of each three-qubit chain. Once this eigenspectrum is computed for a given coupling strength J, we perform a two-parameter fit on $\Gamma(s)$ and $\mathcal{J}(s)|J|$ in equation (1), minimizing a weighted average of the differences in the first eight eigengaps between the qubit Hamiltonian and the transverse-field Ising Hamiltonian. The effective qubit temperatures were measured using standard single-qubit susceptibility measurements.

Fermionized models and TEBD. Calculations using the fermionized system were performed on the same number of spins as in QA, that is, L=512 (Fig. 3) and a range of L (Fig. 4). The TEBD data in Fig. 3 were produced using L=256 to reduce the computation time. This has a negligible effect on the results since this is much larger than the correlation length at the values of t_a investigated, as we confirmed by solving the fermionized model at both L=256 and L=512. The average and

error bars representing 95% statistical confidence in the TEBD data were obtained for 300 realizations of disorder.

Data availability

Data supporting the findings of this paper are available from the corresponding author upon request. Source data are provided with this paper.

Code availability

The TEBD code used in this paper is available from the corresponding author upon reasonable request. An open-source version of the PIMC code used in the Supplementary Information is available via GitHub at https://github.com/dwavesystems/dwave-pimc. The version for this work is archived in Zenodo at https://doi.org/10.5281/zenodo.6842260.

Acknowledgements

We thank H. Oshiyama, N. Shibata, A. del Campo, L. Addario-Berry, T. Albash and A. W. Sandvik for fruitful discussions, and acknowledge the contributions of both technical and non-technical staff at D-Wave. We acknowledge the Center for Advanced Research Computing (CARC) at the University of Southern California for providing computing resources that have contributed to the research results reported within this publication. URL: https://carc.usc.edu. DAL acknowledges support from the National Science Foundation the Quantum Leap Big Idea' under Grant No. OMA-1936388, and by DARPA under the RQMLS program, Agreement No. HR00112190071.

Author contributions

A.D.K., S.S., J.R., A.Z., T.L. F.A., A.J.B., S.E., R.H., D.A.L., H.N. and M.H.A. conceived and designed the experiments and analysed the data. A.D.K., S.S., J.R., A.Z., T.L. and R.H. performed the experiments. T.L., F.A., A.J.B., S.E., E.H., S.H., E.L., A.J.R.M., G.M., T.O., G.P.-L., M.R., C.R., Y.S., J.D.W., J.Y., R.H. and M.H.A. contributed to the design, fabrication, deployment and calibration of the quantum annealing system. A.D.K., S.S., J.R., D.A.L., H.N. and M.H.A. wrote the manuscript.

Competing interests

S.S., D.A.L. and H.N. declare no competing interests. A.D.K., J.R., A.Z., T.L., F.A., A.J.B., S.E., E.H., S.H., E.L., A.J.R.M., G.M., T.O., G.P.-L., M.R., C.R., Y.S., J.D.W., J.Y., R.H. and M.H.A. affiliated with D-Wave hold stock options in D-Wave and declare a competing financial interest on that basis.

Additional information

Supplementary information The online version contains supplementary material available at https://doi.org/10.1038/s41567-022-01741-6.

Correspondence and requests for materials should be addressed to Andrew D. King.

Peer review information *Nature Physics* thanks Guglielmo Mazzola, David Bernal Neira and the other, anonymous, reviewer(s) for their contribution to the peer review of this work.

Reprints and permissions information is available at www.nature.com/reprints.